

Published in final edited form as:

Nat Genet. 2018 October ; 50(10): 1375–1380. doi:10.1038/s41588-018-0211-z.

Promoter capture Hi-C based identification of recurrent non-coding mutations in colorectal cancer

Giulia Orlando^{#1}, Philip J. Law^{#1}, Alex J. Cornish^{#1}, Sara E. Dobbins¹, Daniel Chubb¹, Peter Broderick¹, Kevin Litchfield¹, Fadi Hariri², Tomi Pastinen^{2,3}, Cameron S. Osborne⁴, Jussi Taipale^{5,6,7}, and Richard S. Houlston¹

¹Division of Genetics and Epidemiology, The Institute of Cancer Research, London, UK ²McGill University and Genome Quebec Innovation Centre, Department of Human Genetics, McGill University, Montreal, Quebec, Canada ³Center for Pediatric Genomic Medicine, Children's Mercy, Kansas City, MO, USA ⁴Department of Medical and Molecular Genetics, King's College London, London, UK ⁵Division of Functional Genomics and Systems Biology, Department of Medical Biochemistry and Biophysics, and Department of Biosciences and Nutrition, Karolinska Institutet, Stockholm, Sweden ⁶Genome-Scale Biology Program, University of Helsinki, Biomedicum, Helsinki, Finland ⁷Department of Biochemistry, University of Cambridge, Cambridge, UK

These authors contributed equally to this work.

Abstract

Efforts are being directed to systematically analyse the non-coding genome for cancer-driving mutations^{1–6}. *Cis*-regulatory elements (CREs) represent a highly enriched subset of the non-coding genome in which to search for such mutations. We use capture Hi-C for 19,023 promoter fragments to catalogue the regulatory landscape of colorectal cancer (CRC) in cell lines, mapping CREs and integrating these with TCGA whole genome sequence and expression data^{7,8}. We identify a recurrently mutated CRE interacting with the *ETV1* promoter affecting gene expression. *ETV1* expression influences cell viability and is associated with patient survival. We further refine our understanding of the regulatory effects of copy-number variations (CNVs), showing *RASL11A* to be targeted by a previously identified enhancer amplification¹. This study reveals

Correspondence to: Richard S Houlston; Tel: +44(0) 208 722 4175, Fax: +44(0) 208 722 4365, richard.houlston@icr.ac.uk.

Data Availability

Hi-C, CHi-C, and histone ChIPseq sequencing data have been deposited in the European Genome-phenome Archive (EGA) under the accession code EGAS00001001946. WGS, RNAseq, CNV and survival data for TCGA COAD and READ samples, and RNAseq data for HT29 and LoVo (CCLE program) were obtained from the NCI Genomic Data Commons Data Portal (see URLs). TF ChIPseq data were obtained from the Gene Expression Omnibus (GEO) (GSE49402). Survival data were obtained from GEO (GSE33113, GSE39582). Replication timing data were downloaded from the UCSC Genome Browser (see URLs). GTEx data (release v6) were obtained from the GTEx portal (see URLs).

Author Contributions

G.O., P.J.L., R.S.H. conceived and designed the study; G.O. performed Hi-C and CHi-C experiments, luciferase assays, CRISPR experiments, cell viability and proliferation assays; G.O. and P.B. performed 3C validation; G.O., P.J.L., A.J.C., S.E.D., D.C. and K.L. performed bioinformatics; F.H. performed ChIPseq experiments; T.P. and J.T. contributed reagents and materials for the ChIPseq experiments; C.S.O. designed the capture baits; and G.O., P.J.L., A.J.C., S.E.D., D.C., P.B. and R.S.H. wrote the manuscript with contributions from T.P., C.S.O. and J.T. All authors reviewed the final manuscript.

Competing Financial Interests

The authors declare no competing financial interests.

new insights into the complex genetic alterations driving tumour development, providing a paradigm for employing chromosome conformation capture to decipher non-coding CREs relevant to cancer biology.

The identification of driver mutations as distinguished from passenger mutations is fundamental to understanding cancer and its response to therapy. With the large number of exome-sequenced tumours, all genes with coding changes that contribute substantially to tumourigenesis are likely to be catalogued shortly. Motivated by the identification of recurrent mutations in regulatory elements in genes associated with oncogenesis, such as the *TERT* promoter^{9,10}, and *TAL1*¹¹ and *PAX5*¹² enhancers, efforts are now being directed to systematically analyse non-coding regions of cancer genomes for driver mutations^{1–6}.

Although regional excess of somatic mutations is suggestive of positive selection in tumours, the size of the non-coding genome places a high burden on robustly establishing statistical significance. Coding regions provide obvious, discrete intervals in which to search for mutations, and it would be highly propitious to define similar functional elements for non-coding regions. CREs modulating gene expression represent a highly-enriched subset of the non-coding genome in which to search for driver mutations. These CREs however, can be highly tissue-specific, are often dispersed over long ranges, and only a small fraction of distal enhancers target the nearest transcript^{8,13}. The recent development of high-throughput chromosome conformation capture techniques (Hi-C) has allowed researchers to map such regulatory regions, and importantly, link these to their respective target genes^{8,14–16}.

Here we have used capture Hi-C (CHi-C) for 19,023 promoter fragments to catalogue the CRE landscape of CRC, identifying putative enhancers^{8,16}. Using these data in conjunction with TCGA whole genome sequencing (WGS), RNA sequencing (RNAseq) and CNV data⁷, we report the identification of novel non-coding driver mutations for CRC (Fig. 1, Supplementary Fig. 1, Supplementary Note).

We prepared *in situ* HindIII-digested Hi-C libraries from CRC HT29 and LoVo cell lines, which represent the two major molecular subtypes of CRC – microsatellite stable (MSS) and microsatellite instable (MSI), respectively. To examine the interactions underlying CREs in CRC, we generated a biotinylated RNA bait library, specifically targeting 19,023 promoter-encompassing HindIII fragments representing 2.3% of all HindIII fragments. We hybridised *in situ* Hi-C libraries to the RNA baits to capture promoter-associated di-tags and sequenced the resulting libraries, from which we identified 96,458 and 118,758 significant contacts in LoVo and HT29 respectively (Supplementary Tables 1-3). In both cell lines, the majority of interactions were within topologically associated domains (TADs) (74% and 83% in HT29 and LoVo, respectively; Supplementary Tables 4 and 5, Supplementary Note). Across 127 cell lines and tissues¹⁷ the LoVo and HT29 CREs showed strong enrichment of histone marks identified in colonic tissue (Supplementary Table 6).

The CREs identified by CHi-C were evolutionally conserved ($P < 1.0 \times 10^{-3}$) and enriched for transcription factor (TF) binding as compared to a random set of genomic fragments (3-fold and 2-fold enrichment for HT29 and LoVo respectively, $P < 1.0 \times 10^{-3}$; Supplementary Fig. 2).

Based on the level of gene expression using RNAseq for respective target genes we classified interactions as either active or inactive. As previously documented⁸, a higher frequency of interactions and shorter contact distances typified promoters of active genes (Supplementary Fig. 3). For genes that were actively transcribed, both promoters and their respective CREs had a higher number of bound TFs ($P < 2.2 \times 10^{-16}$; Supplementary Fig. 4). Moreover, a relationship between elevated gene expression and higher proportion of TFs bound to CREs was shown, consistent with the functional role of identified CREs (Supplementary Fig. 5).

To investigate the frequency of single nucleotide variants (SNVs) in CREs delineated by CHi-C we analysed colon and rectal adenocarcinoma WGS data from TCGA⁷. After applying stringent quality control and filtering, we retained data on 50 MSS and 12 MSI cancers. The frequencies of SNV base changes were consistent with those previously documented for CRC^{18,19} (Supplementary Fig. 6, Supplementary Table 7). Both promoters and CREs showed a significantly lower rate of mutation compared to the genome rate in MSS and MSI cancers (Fig. 2). This property was also seen after taking into account mutational-signature-derived substitution probabilities (Fig. 2). This is consistent with previous reports that have shown that functional regulatory regions are less likely to be mutated than non-functional regions of the genome, either as a consequence of selective evolutionary pressure or chromatin accessibility^{9,20}. Since MSI cancers exhibit a significantly higher mutational rate to MSS cancers (median mutations 92,968 and 14,290, respectively) reflective of mismatch repair deficiency¹⁹ (Supplementary Table 8), we analysed the two CRC subtypes separately.

To identify non-coding driver mutations in CREs, we integrated results from three driver discovery methods (Supplementary Fig. 7a). First, we assessed the transcriptional affects of CRE mutations by comparing the expression levels of respective target genes in mutated and non-mutated cancers^{9,10,21}. To avoid confounding, cancers in which either the CRE or target gene were subject to CNVs were excluded from the analysis. Second, we tested for regional excess of mutations to provide evidence of positive selection^{6,9,21,22}. Third, we assessed the clustering of CRE mutations, as this can be suggestive of events in specific TF binding sites²¹. In MSS cancers this integrated analysis yielded a CRE interacting with the *ETVI* promoter, associated with differential target gene expression and an excess of clustered mutations (Fig. 3a-b, Supplementary Tables 9 and 10). Conversely, no CREs were identified in MSI cancers, and we therefore restricted further SNV analysis to MSS cancers.

We demonstrated the benefit of using CHi-C data to discover non-coding driver mutations by comparing the number of CREs identified by the integrated driver discovery analysis using real and randomised CHi-C data. Specifically, we randomised the CHi-C data by changing the HindIII fragments contacting each gene, sampling from non-interacting fragments within 1Mb of the gene, whilst maintaining the number of fragment contacts (Supplementary Fig. 7b), and applied the integrated driver discovery analysis in full to each randomised CHi-C data set. Through this procedure we estimated the empirical false discovery rate (FDR) for the *ETVI* CRE to be 0.023 (Supplementary Table 9, Supplementary Fig. 8).

ETV1, an oncogene encoding an ETS TF, is altered in several cancers by translocations in Ewing's sarcoma²³ and prostate cancer^{24,25}, amplification in melanoma²⁶, and oncogenic dysregulation in gastrointestinal stromal tumours^{27,28}. The *ETV1* interaction was confirmed in a panel of MSS CRC cell lines (Supplementary Fig. 9). Considering only the five cancers without a structural variation (SV) within 1 Mb from *ETV1* (Supplementary Table 11), CRE mutations were associated with a 4-fold increased expression of *ETV1* compared to non-mutated samples (Fig. 3b). Additionally, increased *ETV1* expression was also seen in two cancer samples without CRE mutations but with *ETV1* amplifications ($P=4.1\times 10^{-3}$; Supplementary Fig. 10a). Four of the six mutations map proximally to an evolutionary conserved region (Fig. 3a), and in HT29 each was associated with a 3-fold increase in luciferase activity, consistent with regulatory impact (Fig. 3c, Supplementary Figure 10b). The *ETV1* CRE, which is proximal to an enhancer H3K4me1 chromatin mark, uniquely interacts with the *ETV1* promoter, and the contact is not present in LoVo or 17 blood-specific ChI-C data (Fig. 3a, Supplementary Fig. 11). While the putative enhancer maps within the intron of *DGKB*, there was no relationship between CRE mutation and *DGKB* expression (Supplementary Fig. 12). Although no TF was bound to the CRE on the basis of HT29 cell line ChIPseq data, *in silico* analysis identified numerous potential disrupted TF binding sites^{29–31} including those for BCL6, HNF1A, HNF1B and MAFK, all of which are expressed in colonic tissue³² (Supplementary Table 12 and 13, Supplementary Fig. 13, Supplementary Note).

We made use of Affymetrix SNP Array 6.0 data from 615 TCGA CRC samples to identify CREs subject to somatic CNVs. CNV-positive CREs were assessed for correlation with expression of their interacting gene, where it was not encompassed by the same CNV, using matched RNAseq data. The *RASL11A* promoter showed interactions with a putative enhancer characterised by H3K4me1 marks in both HT29 and LoVo cell lines (Fig. 4a, Supplementary Fig. 14). While a role for *RASL11A* in tumorigenesis has yet to be defined, it is reported to be a GTPase chromatin-associated modulator of pre-ribosomal RNA synthesis, acting to facilitate initiation of transcription by RNA polymerase 133. The *RASL11A* interaction was confirmed in a panel of MSS CRC cell lines (Supplementary Fig. 9). This CRE was amplified in 12 cancer samples and these had significantly higher *RASL11A* expression ($P=2.96\times 10^{-11}$; Fig. 4b, Supplementary Table 14). Using CRISPR-mediated genome editing, disruption of the interacting CRE was shown to reduce *RASL11A* expression (Fig. 4c and 4d, Supplementary Fig. 15). *USP12* has previously been implicated as a target of this specific CRE1. However, after exclusion of samples in which CNVs overlay the gene itself, amplification of the CRE was not associated with differential expression of *USP12* or any other gene in the proximity of the CNV segments (Fig. 4e, Supplementary Table 15).

In HT29, reduction of endogenous *ETV1* and *RASL11A* levels using siRNA was associated with decreased cell viability and cell proliferation (Fig. 5, Supplementary Fig. 16, Supplementary Note). Using patient outcome data from three independent series totalling 1,282 CRC cases^{7,34,35}, high levels of *ETV1* expression were associated with worse relapse-free and overall survival in a multivariate analysis. Respective meta-analysis hazard ratios associated with elevated expression were 1.32 (95% confidence interval [CI]: 1.06-1.64, $P=1.5\times 10^{-2}$) and 1.14 (95% CI: 1.03-1.27, $P=9.9\times 10^{-3}$) (Supplementary Fig. 17,

Supplementary Table 16, Supplementary Note). No significant association was shown between *RASL11A* expression and patient outcome, although data were not available for all series (Supplementary Table 16).

It is arguable that despite high-profile, genuine successes, the number of new driver genes from exome sequencing projects has been disappointingly small compared with expectations. Many cancers have no observable driver mutation, and the full complement of molecular lesions that are individually necessary, and together sufficient, to cause malignancy are still unknown. The Encyclopedia of DNA Elements (ENCODE) project has proposed that around 80% of the genome contains elements linked to biochemical functionality³⁶, however others have estimated that the percentage of the human genome that is functional may actually be 10-fold lower³⁷. Hence, rather than exploiting the epigenomic landscape we identified physical contacts between promoters and the interacting CREs, thereby reducing the genomic space in which to search for non-coding driver mutations.

In our analysis, we identified a CRE whose mutation was associated with altered expression in CRC. This CRE, interacting with the *ETVI* promoter, was mutated in 12% of MSS cancers with mutation being associated with significant upregulation of *ETVI* expression. While not previously assessed as a determinant of CRC outcome³⁸, upregulation of *ETVI* was seen to be associated with poor patient prognosis in CRC (Supplementary Fig. 17, Supplementary Table 16). The fact that upregulation of *ETVI* has previously been linked to reduced survival in other cancers, including gastric cancer, is therefore entirely consistent with increased *ETVI* expression inducing aberrant activation of transcriptional programs that generically governs multiple facets of tumorigenesis. In addition to SNVs having a role in dysregulation of gene expression, we have provided evidence that implicates *RASL11A*, through amplification of an interacting CRE, in CRC oncogenesis.

We acknowledge that the present analysis has limitations. Firstly, we have used a cellular model to map the CREs, which is unlikely to fully recapitulate the spectrum of pathogenic SNVs and CNVs seen in CRC. Secondly, the low-resolution of the defined CNVs has not permitted the study of smaller structural changes, potentially affecting the discovery of deleted or amplified CREs. Thirdly, inevitably as our WGS dataset is modest, this has restricted the study power to identify non-coding drivers. Fourthly, our strategy may not identify genes that are up or down regulated in most cancers, either when driven by the same or alternative mechanisms.

Accepting these caveats, the generation of a genome-wide promoter-CRE map of CRC using *in situ* CHi-C has allowed us to perform a highly focused search for functional non-coding mutations. As sequencing costs are significantly reduced, this will afford the opportunity to perform CHi-C directly on respective WGS samples, thereby providing the opportunities to define individualised networks.

In conclusion, our work supports the existence of non-coding drivers for CRC, and more broadly provides a paradigm for employing chromosome conformation capture to decode disease-specific regulatory elements. Such discoveries facilitate the identification of novel

therapeutic and chemoprevention agents, and classification of patients into molecular subgroups to personalise therapy. For example, it allows for the repositioning of *ETVI* inhibitors, one of which has been employed in a clinical trial for gastrointestinal stromal tumours^{28,39}.

Online Methods

Cell culture

HT115 and SW948 were obtained from ECACC, and all other cell lines were obtained from ATCC. All cell lines were cultured at 37°C; LoVo was cultured in Ham's F-12 Nutrient Mix, HT29 was cultured in McCoy's 5A (Modified) medium, SW480 and SW1116 were both cultured in DMEM, SW948 were cultured in Leibovitz's L-15, all supplemented with 10% FBS. Caco2 was cultured in MEM supplemented with 20% FBS, HT115 was cultured in DMEM supplemented with 15% FBS. Cell line identity was confirmed by STR-profiling. Cells were regularly tested for mycoplasma contamination (PromoCell, PK-CA91).

Hi-C analysis

***In situ* Hi-C library preparation**—*In situ* Hi-C libraries were prepared as previously described^{14,16}. Briefly, 25 million cells were fixed in 1% formaldehyde for 10 min. Cross-linked DNA was digested by restriction enzyme HindIII (NEB, R0104). Digested chromatin ends were filled and marked with biotin-14-dATP (ThermoFisher, 19524-016). The resulting blunted ended fragments were ligated at 16°C in the nucleus with T4 DNA ligase (NEB, M0202) to minimise random ligation. DNA purified after crosslinking was reversed by proteinase K (Ambion, AM2546) treatment. DNA was sheared by sonication (Covaris, M220) and 200-650bp fragments selected. Biotin tag DNA was pulled down with streptavidin beads and ligated with Illumina paired end adapters (Illumina). Six cycles of PCR were performed to amplify libraries before capture.

Promoter capture Hi-C library—Promoter capture was based on 32,313 biotinylated 120-mer RNA baits (Agilent Technologies) targeting both ends of HindIII restriction fragments that overlap Ensembl promoters of protein-coding, non-coding, antisense, snRNA, miRNA and snoRNA transcripts⁸ (Supplementary Table 17). After library enrichment, a post-capture PCR amplification step was carried out using 5 amplification cycles. Hi-C and ChI-C libraries were sequenced using HiSeq 2000 technology¹⁶ (Illumina).

Interaction calling—Reads were aligned to the GRCh37 build using Bowtie2 v2.2.640 and identification of valid di-tags was performed using HiCUP v0.5.941. To declare significant contacts, HiCUP output was processed using CHiCAGO v1.1.842. For each cell line, data from three independent biological replicates were combined to obtain a definitive set of contacts. As previously advocated, interactions with a score ≥ 5.0 were considered to be statistically significant⁴².

ChIPseq analysis

ChIPseq was performed on H3K4me1, H3K9me3, H3K27me3 and H3K36me3 for LoVo, and H3K4me1 and H3K9me3 for HT29. Description of the procedures performed can be found in the Supplementary Note.

Gene expression in LoVo and HT29

Analysis of RNAseq data on LoVo and HT29 cell lines was performed as previously described⁷. Briefly, RNAseq BAM files were downloaded from the Broad Institute Cancer Genomics Hub and analysed using Cufflinks⁴³. Gene-level FPKM read counts were derived using GENCODE v7 annotated mRNA transcripts. Genes with FPKM >0 were divided into quartiles based on their expression levels, with genes with either 0 FPKM or in Q1 considered to be inactive, and genes in Q2-Q4 considered to be active^{8,44}. For promoter fragments associated with multiple genes, we excluded those with discordant expression.

Annotation of *cis*-regulatory elements in LoVo and HT29

Reads that did not align uniquely were removed by HiCUP as they are liable to result in false positive contacts. The detection of duplicate regions is dictated by genomic build. Therefore, an additional filtering step was performed to remove contacts between fragments mapping to regions that did not map to unique locations in hg38. Briefly, hg19/GRCh37 was split into windows of 100bp before being aligned to hg38 using BWA. A base was considered to be poorly mapped if the majority of reads containing it could be mapped elsewhere in the genome with at most one mismatch or gap, as described in SNPable (see URLs). A contact region was kept if 95% of its constituent bases were not poorly mapped imposing this metric. Conservation was measured using PhastCons 100way, considering the average conservation score in 100bp windows centred on each mutation⁴⁵. The proportion of CREs, not overlapping any coding regions, containing runs of at least 8 conserved sites (defined by PhastCons score >0.5) was compared for the set of LoVo and HT29 CREs to sets of randomly generated fragments. For enrichment calculations, random non-coding regions of the genome were selected matching the identified CREs in fragment size and number, restricting start positions to HindIII sites. Random fragments not overlapping coding regions were resampled 1,000 times. Significance was determined by permutation. We annotated each CHI-C contact identified in LoVo and HT29 cells with chromatin features and TF binding information. HindIII interacting fragments were overlaid with histone marks from 127 tissues and cell lines from the ROADMAP Epigenomics project¹⁷ and ChIPseq experiments⁴⁶ (198 and 29 experiments in LoVo and HT29 respectively). Enrichment calculations were performed as described above. The activity of each promoter on its corresponding gene was defined as active or inactive based on the analysis of the matching RNAseq data. To assess whether there was a relationship between TF binding and expression, we selected only the fragments that interact with promoters of genes belonging to the same expression quartile and allocated TF counts to each CRE as previously described⁸. For promoter fragments associated with multiple genes, all genes' expression

URLs

SNPable, <http://bit.ly/snpable>; NCI Genomic Data Commons Data Portal, <https://portal.gdc.cancer.gov/>; UCSC Genome Browser, <http://hgdownload.cse.ucsc.edu/goldenPath/hg19/encodeDCC/wgEncodeUwRepliSeq/>; GTex portal, <https://gtexportal.org/>.

was required to be in the same expression quartile. For each expression class, we calculated the proportion of CREs bound by the TF divided by the proportion of all the CREs bound by the same TF. Corresponding values were \log_2 transformed^{8,44}.

TCGA colorectal cancer whole genome sequencing data

Whole-genome sequencing (WGS) data on 50 MSS (36 colon adenocarcinoma [COAD] and 14 rectal adenocarcinoma [READ]) and 12 MSI were obtained from TCGA. Description of these data and mutation calling can be found in the Supplementary Note.

Mapping non-coding mutations to chromatin-looping interactions

We mapped non-coding mutations to CREs defined by promoter CHi-C generated on CRC cell lines, LoVo and HT29. We annotated only *cis*-interactions involving a promoter and CRE, excluding *trans*-interactions and promoter-promoter contacts.

Genome-wide analysis of non-coding mutations

Mutations were allocated to promoters or CREs, and the mutation rates for each fragment class were calculated. Mutation rates were determined as the number of mutations in each fragment class, divided by the size of all the fragments in that class, minus all regions overlapping ORFs, 3' UTRs, 5' UTRs and regions with poor mappability (Supplementary Note). Mutational signatures have however been shown to be critical for estimating purifying selection pressures in cancer somatic mutation data⁴⁷. Taking this into account the expected mutation rates were estimated considering the sample-specific occurrence of mutations of each of the 96 substitution types defined by Alexandrov *et al.*¹⁸, and the trinucleotide composition of the fragment class.

$$\text{Expected mutation rate} = \frac{\sum_i u_i w_i / v_i}{y}$$

$$i \in (A[C > A]A, \dots, T[T > G]T)$$

where i is each of the possible mutation substitutions, u_i is the genome-wide number of mutations of type i , v_i is the genome-wide number of positions at which mutations of type i can occur, w_i is the number of positions in the considered fragment class at which mutations of type i can occur, and y is the size of all fragments in the class. Excluded regions as defined above were not considered.

Integrated analysis of non-coding mutations in CREs

To identify potential non-coding driver mutations we integrated three driver discovery methods (Supplementary Fig. 7a). In this integrated analysis, we (i) assessed the transcriptional effects of non-coding mutations in CREs, and (ii) tested for an excess of non-coding mutations in CREs. P -values computed in these two analyses were adjusted for multiple testing using the Benjamini-Hochberg procedure and CREs excluded if $Q \geq 0.05$ in either analysis. Finally we (iii) assessed the clustering of non-coding mutations in the remaining CREs. P -values computed in this clustering analysis were adjusted for multiple

testing using the Benjamini-Hochberg procedure and CREs excluded if $Q \geq 0.05$. These three driver discovery methods are outlined below.

Testing the transcriptional effects of non-coding mutations in CREs—Gene expression profiles were based on RNA sequencing of 12 MSI and 50 MSS CRC cases obtained from TCGA that had matched WGS data (normalised gene-level values, accessed 20 January 2017). Differences between samples analysed on Genome Analyzer and HiSeq were batch-corrected using the ComBat method⁴⁸. To reduce spurious long distance contacts, interactions were filtered such that the distance between the promoter and CRE was $< 1\text{Mb}$ ⁴⁹. For each CRE, samples were divided between non-mutated and mutated based on the presence of non-coding mutations in the corresponding CRE. We tested for differential gene expression between mutated and non-mutated groups using a negative binomial model⁹, implemented in edgeR⁵⁰. Samples with copy number alterations at either the gene or the related CRE were excluded⁹. CREs were not tested if gene expression data were not available for the interacting gene, or if the CRE was mutated in fewer than two samples, after the removal of samples with overlapping copy number alterations. CREs observed to interact with the promoters of multiple genes were tested multiple times. Only CREs interacting with protein-coding genes were tested.

Testing for an excess of non-coding mutations in CREs—We tested regions for an excess of non-coding mutations using a global approach, as *per* Weinhold *et al.*⁹. This assumes that the observed number of tumour samples mutated in any specific region follows the binomial distribution, under the null hypothesis that mutations in the region are not under positive selection. As replication timing affects the nucleotide mutation rate, we estimated the mutation rate using data from HeLa, K562, HEPG2, MCF7 and SKNSH cell lines⁵¹. Again as *per* Weinhold *et al.*⁹, we subsetted the genome into 100kb bins and derived mean replication times for each cell line across each bin. For each interacting region, we then computed a single replication time for each cell line by taking the replication time of the 100kb bin in which the region is located, or the average replication time if the region spanned multiple 100kb bins. For each interacting region, we then identified the top 5% of interacting regions with the most similar replication times across cell lines, measured using the Euclidian distance between the vectors of times. The background nucleotide mutation rate q_i could then be estimated by dividing the number of mutations in this 5% of interacting regions across all samples by the total number of samples with mutation data and the total effective length of the regions. These results are robust to the percentage of interacting regions considered (Supplementary Table 18). We excluded the areas of the interacting regions overlapping ORFs, 3' UTRs, 5' UTRs and areas with poor mappability (Supplementary Note). The removal of these areas is incorporated into the effective lengths of the regions. The estimated sample mutation rate s_i is dependent on the estimated nucleotide mutation rate q_i of the region under the null hypothesis, and the effective size of the region L_i :

$$s_i = 1 - (1 - q_i)^{L_i}$$

Mutational excess P -values follow discreet distributions and we therefore computed randomised P -values for each region i using the right tail masses, as *per Imielinski et al*²²:

$$a_i = P(X \geq k) = 1 - \sum_{j=0}^{k-1} \binom{n}{j} s_i^j (1-s_i)^{n-j}$$

$$b_i = P(X \geq k+1) = 1 - \sum_{j=0}^k \binom{n}{j} s_i^j (1-s_i)^{n-j}$$

$$p_i \sim \text{Uniform}(b_i, a_i)$$

where n is the total number of cancers, k the number of cancers with ≥ 1 mutation in region i and p_i is the corresponding randomised P -value. Inflation factor estimation was conducted with the regression method implemented in the GenABEL R-package⁵². Using all P -values indicated that the statistics generated under this model are weakly inflated ($\lambda_{100\%}=1.08$; Supplementary Fig. 18).

Testing for clustering of non-coding mutations in CREs—We evaluated whether CRE mutations cluster using the weighted average proximity (WAP) method²¹:

$$\text{WAP} = \sum_{i \neq j} e^{-\frac{d_{i,j}^2}{2t^2}}$$

where d is the linear genomic distance between mutations i and j , and t is a weighting constant. As *per Rheinbay et al*²¹, we used $t=6$, as this reflects the typical size of the core of TF binding motifs. Statistical significance of each WAP score was determined by permuting mutation positions 10,000 times, whilst maintaining the size of the CRE and excluding regions overlapping ORFs, 3' UTRs, 5' UTRs and regions with poor mappability (Supplementary Note). Empirical P -values were calculated as the proportion of mutation permutations with WAP scores at least as great as the WAP score computed using the observed mutation positions.

Empirical FDR estimation

We estimate an empirical FDR for the identified CRE by comparing the number of results yielded by the integrated driver discovery analysis when using real and randomised CHi-C data (Supplementary Fig. 7b). CHi-C data were randomised by changing the HindIII fragments contacting each gene, by sampling from non-interacting fragments (CHiCAGO score < 1) within 1Mb of the gene, whilst maintaining the number of fragment contacts. The integrated driver discovery analysis was then applied in full to each randomised CHi-C data set. The expected number of false discoveries was estimated as the mean number of CREs yielded by the integrated driver discovery analysis across 1,000 randomised CHi-C data sets. The empirical FDR was estimated as the ratio of false discoveries to the total number of CREs detected when the real CHi-C data were used⁵³.

Relationship between gene expression and CNV at CREs

To identify CNVs overlapping CREs, we utilised Affymetrix Genome-Wide Human SNP Array 6.0 copy number data from the TCGA COAD study of 450 cancers and the READ study of 165 cancers. Focal deletions and amplifications were defined as $\text{abs}(\log_2\text{ratio}) \geq 0.354$ and size $< 3\text{Mb}$. We analysed matched RSEM RNAseq and CNV data from the TCGA COAD and READ studies ($n=606$). To identify cancers with deleted or amplified CREs correlated with expression of an interacting gene, we applied the following filters to each CRE-promoter interaction: (i) we identified cancers with a focal amplification or deletion of the CRE; (ii) we excluded cancers with evidence of a CNV at the interacting gene (a GISTIC2 score $\neq 0$); (iii) we restricted our analysis to CREs affected in ≥ 7 samples (representing 1% of samples). We compared gene expression between affected and unaffected samples using edgeR50 with default parameters. Samples were considered unaffected if there was no evidence of a CNV at the CRE (a GISTIC2 score = 0). Genes that showed differential expression between affected and unaffected samples and an absolute correlation coefficient ≥ 0.4 between GISTIC2 score and gene expression value were taken forward for further analysis.

Relationship between CRE mutation and translocations and inversions

Since translocations and inversions can dysregulate gene expression we examined for translocations and inversions in the proximity of mutated CRE target genes. Translocation and inversion breakpoints, called using dRanger56, were downloaded from the International Cancer Genomic Consortium Data Portal (accessed 30 July 2017).

Genomic DNA extraction

Cells were collected, washed twice in PBS and genomic DNA was extracted using QIAamp DNA Blood Mini Kit (Qiagen). DNA concentration was measured using Qubit dsDNA BR Assay (ThermoFisher Scientific).

3C-PCR validation

3C was used to validate *ETV1* and *RASL11A* interactions in a panel of colon derived MSS CRC cell lines. Two cell culture replicates of *in situ* 3C libraries were prepared using HT29, SW480, SW1116, Caco2, HT115 and SW948 cells. Cell pellets were cross-linked, digested with HindIII, and ligated using the same conditions described in the Hi-C section, excluding the biotin step. Digestion and ligation efficiency were assessed on agarose gel before proceeding to phenol-chloroform purification. Ligation primer pairs were designed to amplify ligation junctions between the promoter and interacting HindIII fragment (promoter-CRE) (Supplementary Table 19). Genomic DNA was used as control for the possibility that amplification across ligation junctions could be the result of structural variations. To prove fidelity of genomic DNA as template, primer pairs were also designed to amplify the genomic region around each of the ligation primers (Supplementary Table 19). All primers were designed using Primer3. Regions were amplified using Multiplex PCR Kit (Qiagen); 100ng template DNA amplified using the following procedure: initial 15 min denaturation at 95°C followed by 38 cycles of 95°C for 30 seconds, 60°C for 90 seconds, 72°C for 45 seconds. 5µl of each PCR reaction was visualised on 2% agarose gels stained with ethidium

bromide. Identity of fragments visualised on agarose gels was confirmed by Sanger sequencing (Supplementary Fig. 9).

Plasmid construction and luciferase assays

The length of the full region spanning the six mutations is over 1.2kb and therefore a 1.6kb fragment would have been required to ensure that all mutations mapped centrally within the fragment. In view of this we decided to clone the two fragments separately, so as to have cloned inserts <1kb. A 946bp and a 738bp genomic region within the *ETVI* CRE were amplified from human genomic DNA using primers detailed in Supplementary Table 19. Gel-purified PCR products (Qiagen) were A-tailed using 2U ThermoPrime DNA polymerase (ThermoFisher Scientific) and 200 μ M dATP for 30 min at 70°C. The products were cloned into the PCR8/GW/TOPO vector and single bacterial colonies containing the vector were cultured and purified (Qiagen Mini-prep Kit). The six somatic mutations were generated with site-directed mutagenesis (SDM) (Agilent Quick Change XL kit) using primers detailed in Supplementary Table 19. SDM changes were confirmed by Sanger-sequencing. Regulatory regions with both non-mutated and mutated sequences were cloned into pGL3 *luc2*-promoter vector (Promega) using Gateway LR Clonase II technology (ThermoFisher Scientific). The reporter constructs were transfected into HT29 using Lipofectamine 2000 (ThermoFisher Scientific). Briefly, 7.5 \times 10⁵ cells were seeded and transfected the following day with 3 μ g reporter constructs and 150ng of internal control plasmid (pRL-TK). Transiently transfected cells were cultured for 24 hours, following which the luciferase assay was performed using the Dual-Luciferase Reporter Assay System (Promega) as per manufacturer's recommendations. Firefly and Renilla luciferase luminescence were measured in triplicate on a Fluoroskan Ascent FL plate reader (ThermoFisher Scientific). The ratio of luminescence from the experimental reporter to the luminescence from the control reporter was calculated for each sample, defined as the relative luciferase activity.

CRISPR-Cas9-mediated enhancer disruption

Two set of guide RNAs (gRNAs) were designed to target the CRE interacting with the *RASL11A* promoter using E-CRISP57. To check that the required PAM sequence was not altered in the HT29 cell line, the region where the gRNAs were mapped was Sanger-sequenced using genomic DNA. Each set of gRNAs was designed to target upstream and downstream of the enhancer region, and cloned in one plasmid expressing the Cas9 gene and the RFP-marker. A control plasmid was generated containing all the elements of the targeting plasmids other than the gRNAs. Custom plasmids were obtained from ATUM. gRNA sequences are reported in Supplementary Table 19. HT29 were seeded at 7.5 \times 10⁵ density in 6-well plates and transfected the following day with 10 μ l of Lipofectamine 2000 (ThermoFisher Scientific) and 2 μ g of the respective plasmids. 48 hours post-transfection cells expressing RFP were selected and seeded into using FACSAriaII μ cell sorter (BD Biosciences) in a 24-well plate. After 2-3 weeks cells were harvested to extract either genomic DNA to confirm the enhancer deletion, or total RNA to assess gene expression. Primers used to assess the deletion are listed in Supplementary Table 19.

Cell viability assays

In 96-well plates, cells were transfected with siRNAs and incubated with Cell Titer Glo reagent according to the manufacturer's protocol (Cell Titer Glo Luminescent Cell Viability Assay kit, Promega). For each experiment, luminescence was measured in triplicate at 0, 24, 48 and 72 hours post-transfection using a Fluoroskan Ascent FL plate reader (ThermoFisher Scientific) (Supplementary Fig. 16).

Real-time cell proliferation assays

After RNAi transfection, 96-well plates were introduced into an Incucyte Zoom imaging system (Essen BioScience) enclosed in an incubator at 37°C and 5% CO₂ humidified air. Each well was imaged by phase contrast every four hours for 92 hours. Images were collected and the percentage of confluence determined using software provided by the manufacturer. Confluence was averaged over four fields of view per well. Data were normalised to the first scan to account for differences in seeding across individual samples and across replicates.

Statistical analyses

The observed and expected mutation rates in promoters and CREs were compared using two-sided paired Wilcoxon tests. CHi-C interactions involving promoters of active and inactive genes were compared using two-sided Wilcoxon tests⁸. For luciferase, cell viability and real-time cell proliferation assays, statistical significance was calculated using two-tailed *t*-tests over three independent experiments. The Benjamini-Hochberg procedure was used to adjust for multiple testing, unless otherwise specified.

Reporting summary

Further information on our experimental design is available in the Nature Research Reporting Summary document linked to this article.

Supplementary Material

Refer to Web version on PubMed Central for supplementary material.

Acknowledgements

This work was supported by grants from Cancer Research UK grant (C1298/A8362), the European Union Seventh Framework Programme (FP7/2007–2013) under grant 258236 and FP7 collaborative project SYSCOL, all awarded to R.S.H. This publication is supported by COST Action BM1206. CIHR funded Epigenome Mapping Centre at McGill University (EP1-120608), awarded to T.P. We acknowledge the work of The Institute of Cancer Research Tumour Profiling Unit. The results published here are in part based upon data generated by The Cancer Genome Atlas established by the NCI and NHGRI. Information about TCGA and the investigators and institutions that constitute the TCGA research network can be found at <http://cancergenome.nih.gov/>.

References

1. Zhang X, et al. Identification of focally amplified lineage-specific super-enhancers in human epithelial cancers. *Nat Genet.* 2016; 48:176–82. [PubMed: 26656844]
2. Sur I, Taipale J. The role of enhancers in cancer. *Nat Rev Cancer.* 2016; 16:483–93. [PubMed: 27364481]

3. Kim K, et al. Chromatin structure-based prediction of recurrent noncoding mutations in cancer. *Nat Genet.* 2016; 48:1321–1326. [PubMed: 27723759]
4. Weischenfeldt J, et al. Pan-cancer analysis of somatic copy-number alterations implicates *IRS4* and *IGF2* in enhancer hijacking. *Nat Genet.* 2017; 49:65–74. [PubMed: 27869826]
5. Fujimoto A, et al. Whole-genome mutational landscape and characterization of noncoding and structural mutations in liver cancer. *Nat Genet.* 2016; 48:500–9. [PubMed: 27064257]
6. Melton C, Reuter JA, Spacek DV, Snyder M. Recurrent somatic mutations in regulatory regions of human cancer genomes. *Nat Genet.* 2015; 47:710–6. [PubMed: 26053494]
7. The Cancer Genome Atlas Network. Comprehensive molecular characterization of human colon and rectal cancer. *Nature.* 2012; 487:330–7. [PubMed: 22810696]
8. Mifsud B, et al. Mapping long-range promoter contacts in human cells with high-resolution capture Hi-C. *Nat Genet.* 2015; 47:598–606. [PubMed: 25938943]
9. Weinhold N, Jacobsen A, Schultz N, Sander C, Lee W. Genome-wide analysis of noncoding regulatory mutations in cancer. *Nat Genet.* 2014; 46:1160–5. [PubMed: 25261935]
10. Fredriksson NJ, Ny L, Nilsson JA, Larsson E. Systematic analysis of noncoding somatic mutations and gene expression alterations across 14 tumor types. *Nat Genet.* 2014; 46:1258–63. [PubMed: 25383969]
11. Mansour MR, et al. Oncogene regulation. An oncogenic super-enhancer formed through somatic mutation of a noncoding intergenic element. *Science.* 2014; 346:1373–7. [PubMed: 25394790]
12. Puente XS, et al. Non-coding recurrent mutations in chronic lymphocytic leukaemia. *Nature.* 2015; 526:519–24. [PubMed: 26200345]
13. Javierre BM, et al. Lineage-Specific Genome Architecture Links Enhancers and Non-coding Disease Variants to Target Gene Promoters. *Cell.* 2016; 167:1369–1384 e19. [PubMed: 27863249]
14. Rao SS, et al. A 3D map of the human genome at kilobase resolution reveals principles of chromatin looping. *Cell.* 2014; 159:1665–80. [PubMed: 25497547]
15. Jager R, et al. Capture Hi-C identifies the chromatin interactome of colorectal cancer risk loci. *Nat Commun.* 2015; 6
16. Orlando G, Kinnersley B, Houlston RS. Capture Hi-C Library Generation and Analysis to Detect Chromatin Interactions. *Curr Protoc Hum Genet.* 2018:e63. [PubMed: 29979818]
17. Roadmap Epigenomics, C. et al. Integrative analysis of 111 reference human epigenomes. *Nature.* 2015; 518:317–30. [PubMed: 25693563]
18. Alexandrov LB, et al. Signatures of mutational processes in human cancer. *Nature.* 2013; 500:415–21. [PubMed: 23945592]
19. Katainen R, et al. CTCF/cohesin-binding sites are frequently mutated in cancer. *Nat Genet.* 2015; 47:818–21. [PubMed: 26053496]
20. Martincorena I, et al. Universal Patterns of Selection in Cancer and Somatic Tissues. *Cell.* 2017; 171:1029–1041 e21. [PubMed: 29056346]
21. Rheinbay E, et al. Recurrent and functional regulatory mutations in breast cancer. *Nature.* 2017; 547:55–60. [PubMed: 28658208]
22. Imielinski M, Guo G, Meyerson M. Insertions and Deletions Target Lineage-Defining Genes in Human Cancers. *Cell.* 2017; 168:460–472 e14. [PubMed: 28089356]
23. Jeon IS, et al. A variant Ewing's sarcoma translocation (7;22) fuses the *EWS* gene to the *ETS* gene *ETV1*. *Oncogene.* 1995; 10:1229–34. [PubMed: 7700648]
24. Attard G, et al. Heterogeneity and clinical significance of *ETV1* translocations in human prostate cancer. *Br J Cancer.* 2008; 99:314–20. [PubMed: 18594527]
25. Clark JP, Cooper CS. *ETS* gene fusions in prostate cancer. *Nat Rev Urol.* 2009; 6:429–39. [PubMed: 19657377]
26. Jane-Valbuena J, et al. An oncogenic role for *ETV1* in melanoma. *Cancer Res.* 2010; 70:2075–84. [PubMed: 20160028]
27. Chi P, et al. *ETV1* is a lineage survival factor that cooperates with *KIT* in gastrointestinal stromal tumours. *Nature.* 2010; 467:849–53. [PubMed: 20927104]
28. Ran L, et al. Combined inhibition of MAP kinase and *KIT* signaling synergistically destabilizes *ETV1* and suppresses GIST tumor growth. *Cancer Discov.* 2015; 5:304–15. [PubMed: 25572173]

29. Grant CE, Bailey TL, Noble WS. FIMO: scanning for occurrences of a given motif. *Bioinformatics*. 2011; 27:1017–8. [PubMed: 21330290]
30. Kulakovskiy IV, et al. HOCOMOCO: expansion and enhancement of the collection of transcription factor binding sites models. *Nucleic Acids Res*. 2016; 44:D116–25. [PubMed: 26586801]
31. Zhou J, Troyanskaya OG. Predicting effects of noncoding variants with deep learning-based sequence model. *Nat Methods*. 2015; 12:931–4. [PubMed: 26301843]
32. The GTEx Consortium. The Genotype-Tissue Expression (GTEx) pilot analysis: Multitissue gene regulation in humans. *Science*. 2015; 348:648–660. [PubMed: 25954001]
33. Pistoni M, Verrecchia A, Doni M, Guccione E, Amati B. Chromatin association and regulation of rDNA transcription by the Ras-family protein RasL11a. *EMBO J*. 2010; 29:1215–24. [PubMed: 20168301]
34. de Sousa EMF, et al. Methylation of cancer-stem-cell-associated Wnt target genes predicts poor prognosis in colorectal cancer patients. *Cell Stem Cell*. 2011; 9:476–85. [PubMed: 22056143]
35. Marisa L, et al. Gene expression classification of colon cancer into molecular subtypes: characterization, validation, and prognostic value. *PLoS Med*. 2013; 10:e1001453. [PubMed: 23700391]
36. The ENCODE Project Consortium. An integrated encyclopedia of DNA elements in the human genome. *Nature*. 2012; 489:57–74. [PubMed: 22955616]
37. Rands CM, Meader S, Ponting CP, Lunter G. 8.2% of the Human genome is constrained: variation in rates of turnover across functional element classes in the human lineage. *PLoS Genet*. 2014; 10:e1004525. [PubMed: 25057982]
38. Sizemore GM, Pitarresi JR, Balakrishnan S, Ostrowski MC. The ETS family of oncogenic transcription factors in solid tumours. *Nat Rev Cancer*. 2017; 17:337–351. [PubMed: 28450705]
39. Duensing A. Targeting ETV1 in gastrointestinal stromal tumors: tripping the circuit breaker in GIST? *Cancer Discov*. 2015; 5:231–3. [PubMed: 25749973]
40. Langmead B, Salzberg SL. Fast gapped-read alignment with Bowtie 2. *Nat Methods*. 2012; 9:357–9. [PubMed: 22388286]
41. Wingett S, et al. HiCUP: pipeline for mapping and processing Hi-C data. *F1000Res*. 2015; 4:1310. [PubMed: 26835000]
42. Cairns J, et al. CHiCAGO: robust detection of DNA looping interactions in Capture Hi-C data. *Genome Biol*. 2016; 17:127. [PubMed: 27306882]
43. Trapnell C, et al. Transcript assembly and quantification by RNA-Seq reveals unannotated transcripts and isoform switching during cell differentiation. *Nat Biotechnol*. 2010; 28:511–5. [PubMed: 20436464]
44. Schoenfelder S, et al. The pluripotent regulatory circuitry connecting promoters to their long-range interacting elements. *Genome Res*. 2015; 25:582–97. [PubMed: 25752748]
45. Pollard KS, Hubisz MJ, Rosenbloom KR, Siepel A. Detection of nonneutral substitution rates on mammalian phylogenies. *Genome Res*. 2010; 20:110–21. [PubMed: 19858363]
46. Yan J, et al. Transcription factor binding in human cells occurs in dense clusters formed around cohesin anchor sites. *Cell*. 2013; 154:801–13. [PubMed: 23953112]
47. Van den Eynden J, Larsson E. Mutational Signatures Are Critical for Proper Estimation of Purifying Selection Pressures in Cancer Somatic Mutation Data When Using the dN/dS Metric. *Front Genet*. 2017; 8:74. [PubMed: 28642787]
48. Johnson WE, Li C, Rabinovic A. Adjusting batch effects in microarray expression data using empirical Bayes methods. *Biostatistics*. 2007; 8:118–27. [PubMed: 16632515]
49. Grubert F, et al. Genetic Control of Chromatin States in Humans Involves Local and Distal Chromosomal Interactions. *Cell*. 2015; 162:1051–65. [PubMed: 26300125]
50. Robinson MD, McCarthy DJ, Smyth GK. edgeR: a Bioconductor package for differential expression analysis of digital gene expression data. *Bioinformatics*. 2010; 26:139–40. [PubMed: 19910308]
51. Hansen RS, et al. Sequencing newly replicated DNA reveals widespread plasticity in human replication timing. *Proc Natl Acad Sci U S A*. 2010; 107:139–44. [PubMed: 19966280]

52. Aulchenko YS, Ripke S, Isaacs A, van Duijn CM. GenABEL: an R library for genome-wide association analysis. *Bioinformatics*. 2007; 23:1294–6. [PubMed: 17384015]
53. Carter H, et al. Interaction Landscape of Inherited Polymorphisms with Somatic Events in Cancer. *Cancer Discov*. 2017; 7:410–423. [PubMed: 28188128]
54. Mermel CH, et al. GISTIC2.0 facilitates sensitive and confident localization of the targets of focal somatic copy-number alteration in human cancers. *Genome Biol*. 2011; 12:R41. [PubMed: 21527027]
55. Litchfield K, et al. Whole-exome sequencing reveals the mutational spectrum of testicular germ cell tumours. *Nat Commun*. 2015; 6
56. Drier Y, et al. Somatic rearrangements across cancer reveal classes of samples with distinct patterns of DNA breakage and rearrangement-induced hypermutability. *Genome Res*. 2013; 23:228–35. [PubMed: 23124520]
57. Heigwer F, Kerr G, Boutros M. E-CRISP: fast CRISPR target site identification. *Nat Methods*. 2014; 11:122–3. [PubMed: 24481216]

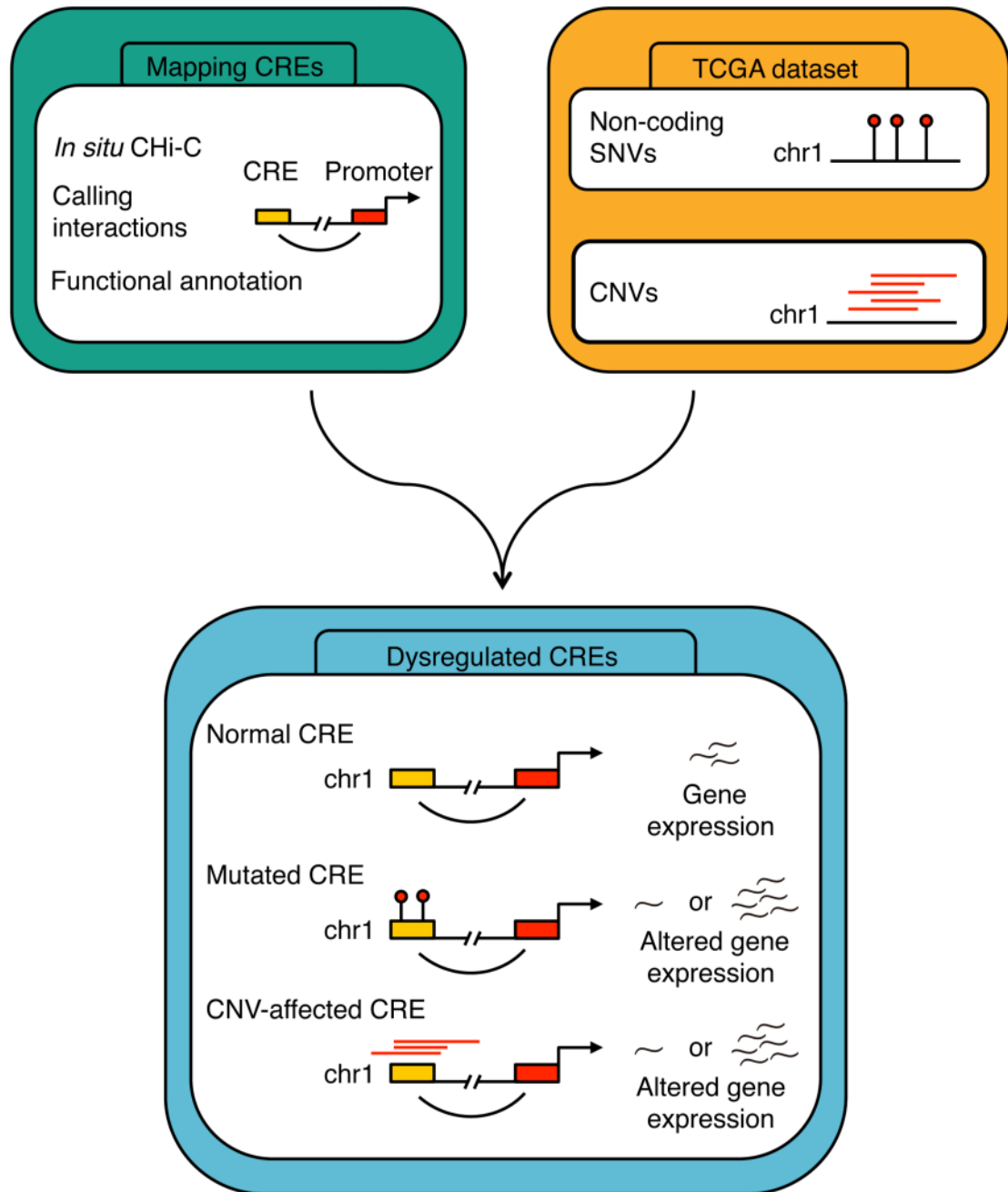


Figure 1. Workflow for the identification of mutated *cis*-regulatory elements in colorectal cancer. CRE, *cis*-regulatory element; SNV, single nucleotide polymorphism; CNV, copy-number variation.

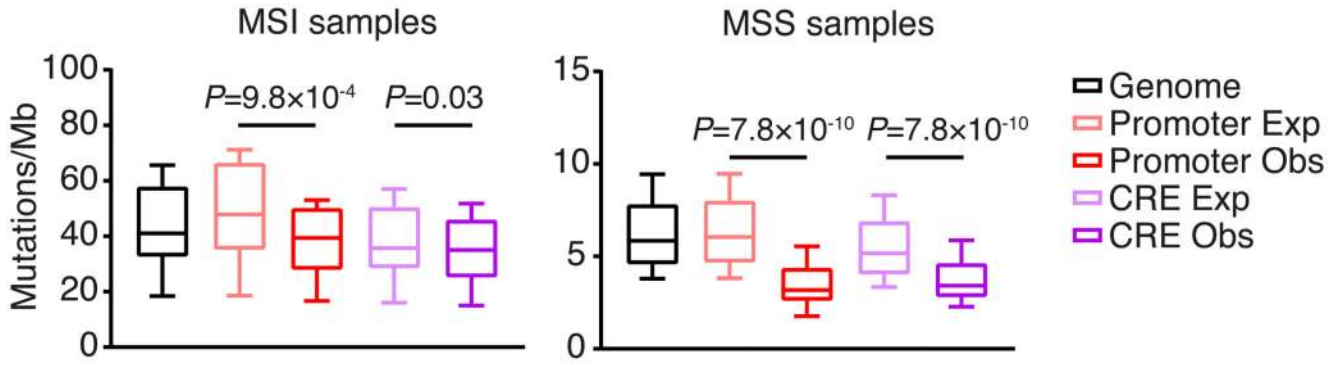


Figure 2. Non-coding mutations in *cis*-regulatory elements.

Mutation rates in promoters, CREs and genome-wide in MSI ($n=12$) and MSS ($n=50$) cancers. Shown are both the mutation rates observed in promoters and CREs, and the mutation rates expected considering the sample-specific occurrence of mutations of each of the 96 substitution types, and the trinucleotide composition of the fragment classes. Box-plots denote quartiles. Whiskers correspond to the 10th and 90th percentiles. Difference assessed using a two-sided paired Wilcoxon test.

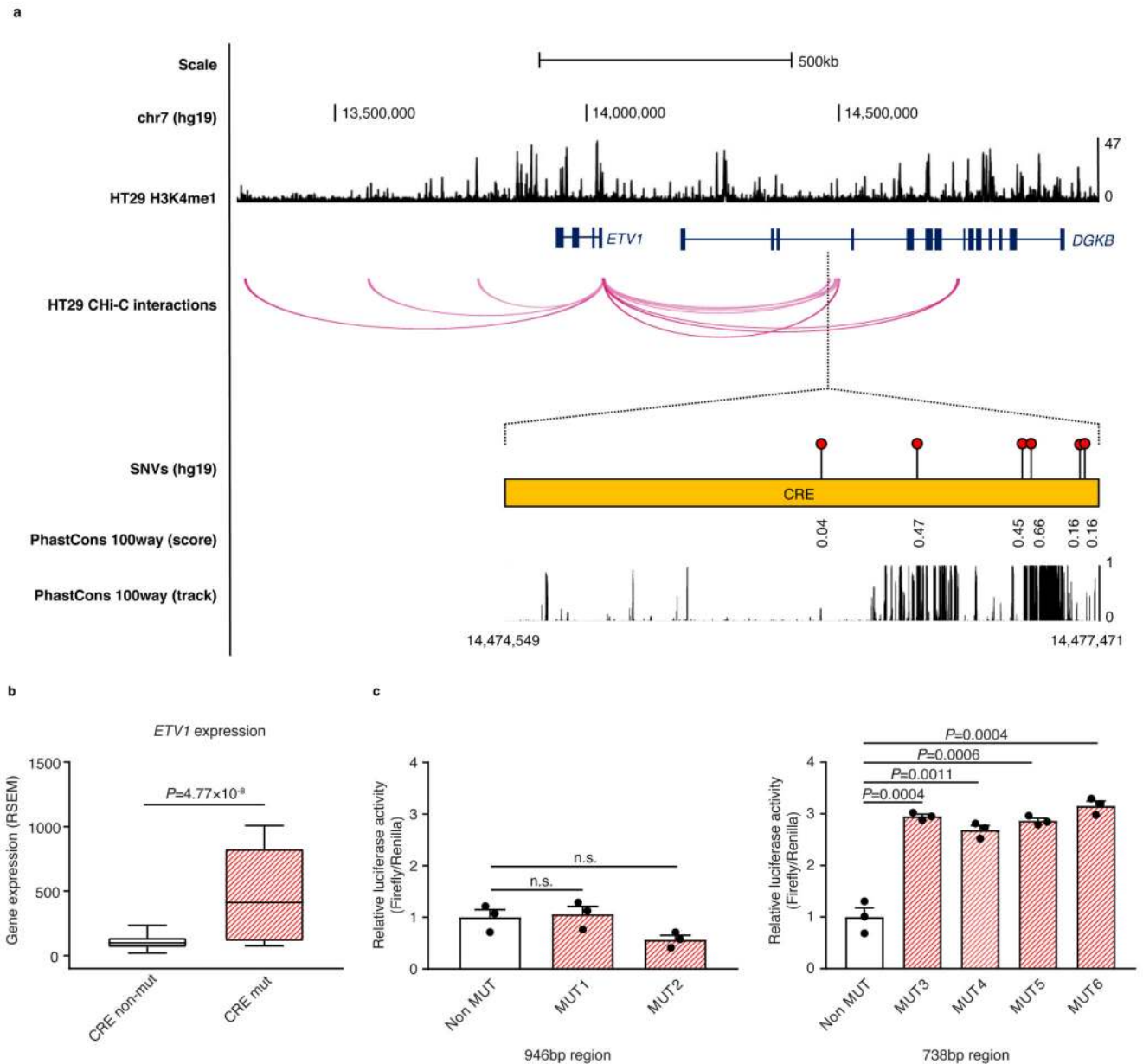


Figure 3. Cis-regulatory element mutation affects *ETV1* expression.

(a) Chromatin looping interactions between the *ETV1* promoter and CREs in HT29. Also detailed are the relative positions of SNVs for the significantly mutated CRE and the evolutionary conservation of the region, as measured using PhastCons 100-way smoothed scores and track. (b) Relationship between mutation status and *ETV1* expression in MSS cancers. One sample containing a CNV overlapping *ETV1* was excluded. Box-plots denote quartiles. Whiskers correspond to the 10th and 90th percentiles. Difference between samples in which the CRE is mutated (mut, $n=5$) and not mutated (non-mut, $n=41$) assessed by negative binomial test. (c) A 946bp and a 738bp putative regulatory regions containing the six mutations were cloned upstream of the SV40 promoter in the pGL3-promoter vector. The resultant reporter constructs were transiently transfected into HT29 for 24 hours and the

relative luciferase activity was measured for each reporter gene construct. The luminescence ratio of the experimental vector to the Renilla internal control, pRL-TK, was normalised to the backbone pGL3-SV40 promoter vector. Data shown are mean \pm SEM relative to the non-mutated (Non MUT) samples from three independent experiments and assessed by two-tailed *t*-test, n.s., non-significant.

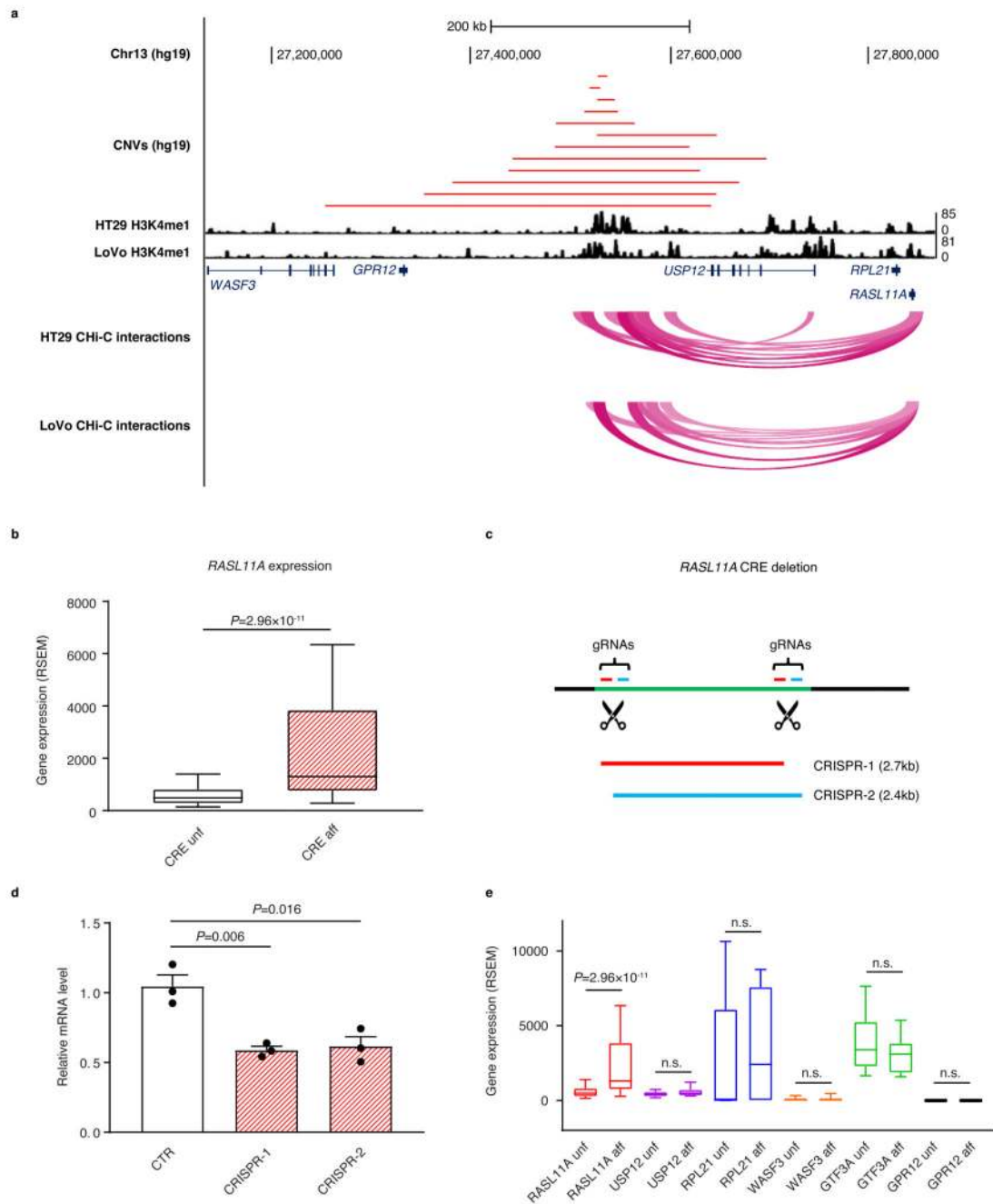


Figure 4. Amplification of *cis*-regulatory element upregulates *RASL11A* expression.

(a) The amplification of the CRE interacting with the *RASL11A* promoter; upper track, CNVs overlapping the CRE in 12 samples; middle track, H3K4me1 mark in HT29 and LoVo; lower track, CHI-C interactions in HT29 and LoVo. (b) *RASL11A* expression in CRC stratified by CRE amplification status (samples with CNV overlapping *RASL11A* excluded). Box-plots denote quartiles. Whiskers correspond to the 10th and 90th percentiles. Difference between samples in which the CRE is affected (CRE aff, n=12) and unaffected (CRE unaf, n=522) by a CNV amplification assessed by negative binomial test. (c) Schematic

representation of the CRISPR/Cas9-mediated deletion using two plasmids expressing different sets of gRNAs. (d) Barplots showing *RASL11A* mRNA levels relative to *GAPDH* in control (CTR) and CRISPR-edited cells (CRISPR-1 and CRISPR-2). Differences assessed by two-tailed *t*-test from three independent experiments, mean \pm SEM. (e) Expression levels of six genes in the proximity of the CRE in the samples where the CRE is affected (aff) or unaffected (unf) by CNV amplification (*RASL11A* unf *n*=522, *RASL11A* aff *n*=12, *USP12* unf *n*=524, *USP12* aff *n*=7, *RPL21* unf *n*=522, *RPL12* aff *n*=12, *WASF3* unf *n*=523, *WASF3* aff *n*=14, *GTF3A* unf *n*=521, *GTF3A* aff *n*=12, *GPR12* unf *n*=523, *GPR12* aff *n*=13). Samples containing CNVs overlapping the respective gene are excluded from each comparison. Box-plots denote quartiles. Whiskers correspond to the 10th and 90th percentiles. Differences assessed by negative binomial test, n.s., non-significant.

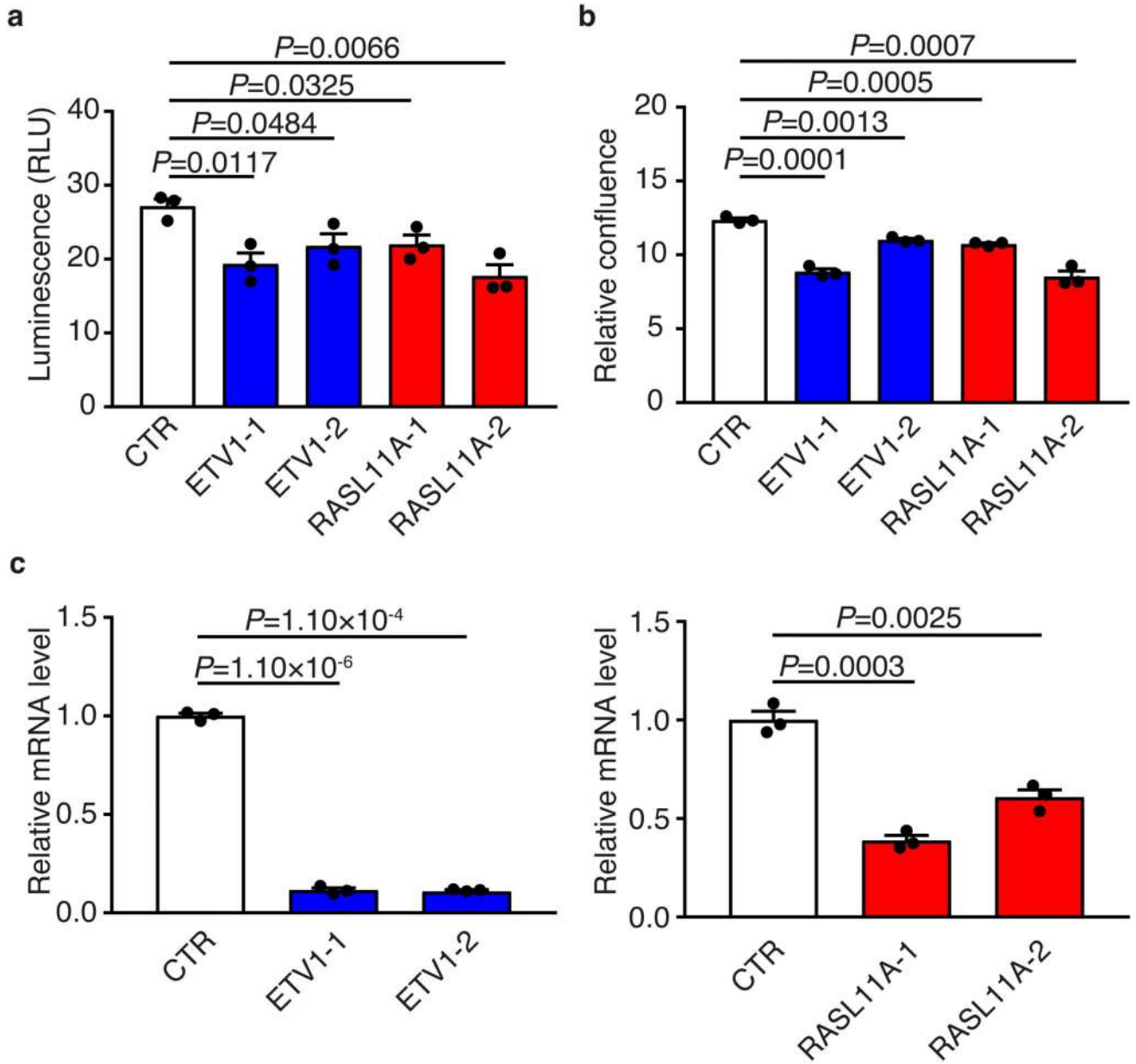


Figure 5. *ETVI* and *RASL11A* levels are associated with differential cell growth.

(a) Relative luminescence of *ETVI*, *RASL11A* and control (CTR) knockdowns. Differences assessed 72 hours post-transfection by two-tailed *t*-test using three independent experiments, mean \pm SEM. (b) Relative confluence of *ETVI*, *RASL11A* and control treated cells. Values normalised to the 0 hour time-point confluence. Differences assessed 96 hours post-transfection by two-tailed *t*-test using three independent experiments, mean \pm SEM. (c) Barplots showing *ETVI* and *RASL11A* mRNA levels, normalised to *GAPDH*, after siRNA treatment. Differences assessed by two-tailed *t*-test using three independent experiments, mean \pm SEM.